

## Orientation of Fluorescent Dyes in the Nano Channels of Zeolite L

Silke Megelski,<sup>†</sup> Andreas Lieb,<sup>‡</sup> Marc Pauchard,<sup>†</sup> Andreas Drechsler,<sup>‡</sup> Stephan Glaus,<sup>†</sup>  
Christina Debus,<sup>‡</sup> Alfred J. Meixner,<sup>\*,‡</sup> and Gion Calzaferri<sup>\*,†</sup>

Department of Chemistry and Biochemistry, Universität Bern, CH-3012 Switzerland, and Physikalische Chemie I, Universität Siegen, D-57068 Germany

Received: July 19, 2000; In Final Form: October 2, 2000

The orientation of the  $S_1 \leftarrow S_0 \pi, \pi^*$  transition dipole moments of oxonine ( $Ox^+$ ), pyronine ( $Py^+$ ), and POPOP (5,5'-diphenyl-2,2'-p-phenylenebis(oxazole)) in the channels of zeolite L crystals was investigated by means of fluorescence microscopy and single-crystal imaging. Qualitative observations led to the result that the transition moment of POPOP is aligned along the  $c$ -axis of the hexagonal crystals whereas the fluorescence of  $Ox^+$  and  $Py^+$  is not. More detailed investigations on  $Ox^+$  showed a cone-shaped distribution of the transition moments with a half-cone angle of  $72^\circ$ . The orientation of the transition dipole moment for all of these molecules is parallel to the molecules' long axis. We found by means of space-filling arguments that POPOP, the van der Waals length of which is about  $21 \text{ \AA}$ , can only be aligned along the channel axis. This is in full agreement with the observed fluorescence anisotropy. For  $Ox^+$  and  $Py^+$ , geometrical arguments based on the zeolite L structure give room for only two possible arrangements of the molecules' long axis: a half cone angle of up to  $40^\circ$  for  $Ox^+$  and up to  $30^\circ$  for  $Py^+$ , and an angle of about  $90^\circ$  for both of them with respect to the  $c$ -axis of zeolite L. The surprising discrepancy between geometrical considerations and the results of the fluorescence measurements can be explained by assuming that  $Ox^+$  and  $Py^+$  are exposed to a considerable anisotropic electrical field in the zeolite channels.

### 1. Introduction

Dyes at high concentration have the tendency to form aggregates. Such aggregates show very fast radiationless decay of electronic excitation in most cases. Their formation can be prevented by fencing the dyes inside a microporous material and by choosing conditions where the volume of the cages and channels allows the uptake of monomers only. Our investigations have been concentrated on zeolite L as a host.<sup>1,2</sup> Zeolite L consists of linear channels running through the crystal. Neutral as well as cationic dyes can be inserted into these channels. Synthesis procedures for controlling the morphology of zeolite L crystals in the size regime from 20 nm to about  $3 \mu\text{m}$  are available.<sup>3–6</sup> We show in Figure 1 an electron microscopy picture of zeolite L. A side view and a space-filling top view of the zeolite L framework are illustrated in Figure 2. The primitive vector  $c$  corresponds to the channel axis while the primitive vectors  $a$  and  $b$  are perpendicular to it, enclosing an angle of  $120^\circ$ .<sup>7–10</sup>

We distinguish between three types of dye molecules that can be inserted into the channels of zeolite L. (i) *Molecules that are small enough to fit into a unit cell.* Examples we have investigated so far are biphenyl, 4-hydroxy-TEMPO, 9-fluorenone, and methyl viologen ( $MV^{2+}$ ). Structural details of the latter are known based on vibrational spectroscopy, Rietveld refinement of X-ray data, and molecular modeling.<sup>11</sup> (ii) *Molecules the size of which makes it hard to guess their position and orientation in the channel.* Oxonine, pyronine, and thionine are molecules of this type.<sup>1,2,12,13</sup> (iii) *Molecules which are so*

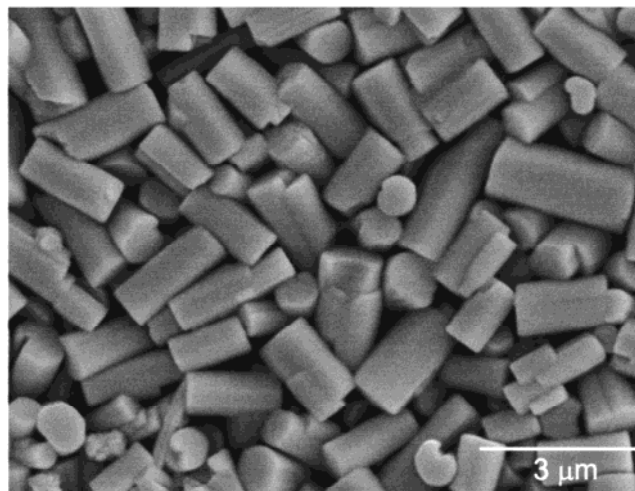


**Figure 1.** Electron microscopy picture of a zeolite L sample consisting of 2–3  $\mu\text{m}$  long crystals.

large that they have no other choice but to align along the  $c$ -axis. Many examples fit into this category. The light-sensitive diphenylhexatriene (DPH) is one of them, which has been studied by us recently.<sup>14</sup> It is dramatically stabilized when inserted into zeolite L, because there is not sufficient space available for trans to cis isomerization. An example investigated here is the so-called POPOP. While for molecules of type (i) not only translational but also large-amplitude modes can be activated, the latter are severely restricted for molecules of type (ii) and (iii). This has consequences on their stability and also on their luminescence quantum yield. In some cases a dramatic increase in stability is observed, because large reactive molecules or anions such as hypochlorite cannot enter the anionic zeolite framework.<sup>1,15</sup>

\* To whom correspondence should be addressed: meixner@chemie.uni-siegen.de, Gion.Calzaferri@iac.unibe.ch.

<sup>†</sup> Universität Bern.

<sup>‡</sup> Universität Siegen.

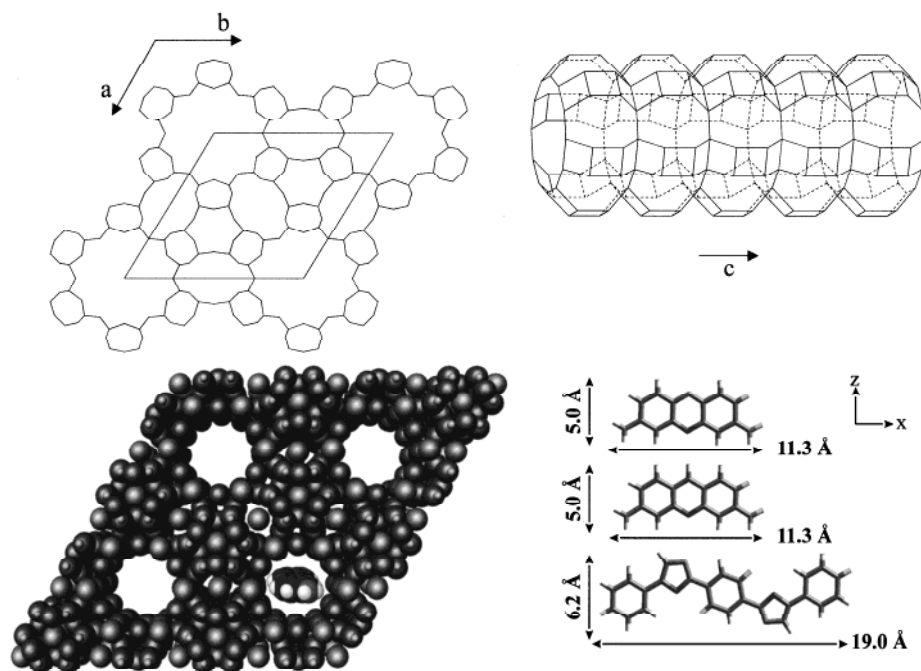


**Figure 2.** Framework of zeolite L. (Left) top view, perpendicular to the *c*-axis, displayed as stick and as van der Waals representation with an oxonine entering the zeolite channel. (Right) Side view of a channel along the *c*-axis, without bridging oxygen atoms, and structure of Ox<sup>+</sup>(top), Py<sup>+</sup>(middle), POPOP (bottom) with atom to atom distances and the coordinate system.

Information about the orientation of the dye molecules inside the nano channels of the zeolite crystals is highly desirable.<sup>1,16,17</sup> Powerful methods such as X-ray and NMR are only accessible to a restricted number of favorable cases, mainly because of their still limited sensitivity. Among the optical methods, fluorescence microscopy is the most sensitive. We present luminescence data on type (iii) dyes that are easy to interpret and on type (ii) dyes, where limits of currently available techniques will be stressed. We first explain some simple geometrical concepts and illustrate information that is accessible by standard optical microscopy techniques. We next present results obtained by polarization dependent imaging of single oxonine loaded zeolite L crystals. Geometrical space-filling arguments illustrating the problems encountered with type (ii) molecules and the consequences of our results are discussed in subsequent sections.

## 2. General

The geometrical constraints imposed by the host determine the organization of the dyes which can be realized. The main channels of zeolite L consist of unit cells with a length of 7.5 Å in the *c*-direction, as illustrated in Figure 2. The unit cells are joined by shared 12-membered ring windows having a free diameter of 7.1–7.8 Å. The largest free diameter is about 12.6 Å, depending on the charge compensating cations.<sup>7,18,19</sup> It lies midway between the 12-membered rings. The lengths of the primitive vectors **a** and **b** is 18.4 Å. A zeolite L crystal of 500 nm diameter and 375 nm length gives rise to about 67 000 parallel channels each of which consists of 500 unit cells, as an example. The dye molecules are positioned at sites along the channels. The length of a site is equal to a number *s* times the length of **c**, so that one dye molecule fits into one site. As an example, a dye of 1.5 nm length requires two primitive unit cells in zeolite L, and hence *s* is equal to 2. Only dye molecules with a large electronic transition moment  $\mu_{S_1-S_0}$  are considered in this account. This means that the  $S_1 \leftarrow S_0$  transition is of  $\pi^* \leftarrow \pi$  type. In homogeneously loaded samples, equivalent sites

have the same probability *p* to be occupied by a dye molecule. The occupation probability *p* is equal to the ratio between the occupied and the total number of equivalent sites. This means that *p* relies on geometrical (space filling) reasoning. Each equivalent site of a given crystal has the same probability of being occupied by an electronically excited molecule, immediately after irradiation with a short pulse.

The dye molecules discussed in this study are shown in Figure 3. We use the abbreviations Ox<sup>+</sup> and Py<sup>+</sup> in order to distinguish these cationic dyes from the neutral POPOP. The spectra of the dyes are slightly different in solution and in the zeolite. It is interesting to observe that the spectra of the two cationic dyes are more structured when they are inside the channels while this is reverse for the neutral POPOP. All dye zeolite samples show very bright luminescence.

## 3. Qualitative Observations

We report some qualitative observations, made by means of a standard optical microscope equipped with polarizers and an appropriate set of filters. A side view of a zeolite L crystal of about 1.5 μm is illustrated in Figure 4. We also show the process of insertion of Py<sup>+</sup> and in a second step Ox<sup>+</sup> into the channels, out of an aqueous suspension of zeolite L crystals containing dissolved Py<sup>+</sup> and Ox<sup>+</sup>, respectively. The zeolite L samples 2–4 were excited with light of 470–490 nm where only Py<sup>+</sup> absorbs. In sample 2 we see how Py<sup>+</sup> penetrates the cylinder from both sides in the direction of the cylinder axis. After an exchange of 5 min under reflux the crystal ends show the typical green fluorescence of Py<sup>+</sup>, while the section in the middle remains dark. The fluorescence is seen over the whole crystal after 2 h exchange, sample 3. The dye molecules have moved toward the center now, but the fluorescence at the ends appears still to be more intense. The result after additional exchange with Ox<sup>+</sup> for 2 h is illustrated in samples 4 and 5. It leads to crystals which show the green fluorescence of Py<sup>+</sup> in the center and the fluorescence of Ox<sup>+</sup> at both ends. The yellow color seen in sample 4 is due to the mixing of the green Py<sup>+</sup> and the

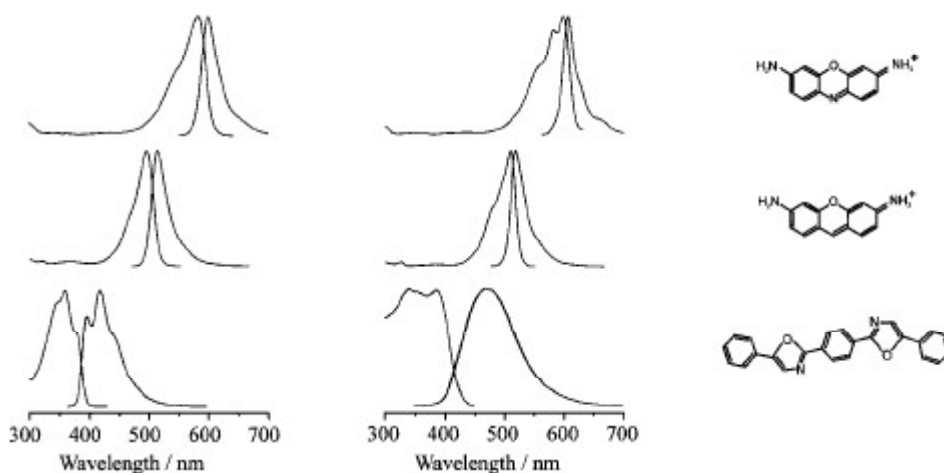


**Figure 3.** Dye molecules investigated and their electronic absorption and fluorescence spectra. From top to bottom: oxonine ( $\text{Ox}^+$ ), pyronine ( $\text{Py}^+$ ), and 5,5'-diphenyl-2,2'-*p*-phenylenebis(oxazole) (POPOP). (Left) Absorption and fluorescence spectra of POPOP (in 1-butanol,  $\lambda_{\text{ex}} = 360$  nm),  $\text{Py}^+$  (in water  $\lambda_{\text{ex}} = 460$  nm), and  $\text{Ox}^+$  (in water  $\lambda_{\text{ex}} = 560$  nm). (Right) Excitation and fluorescence spectra of the same dyes in zeolite L: POPOP ( $\lambda_{\text{em}} = 460$  nm,  $\lambda_{\text{ex}} = 340$  nm),  $\text{Py}^+$  ( $\lambda_{\text{em}} = 560$  nm,  $\lambda_{\text{ex}} = 460$  nm), and  $\text{Ox}^+$  ( $\lambda_{\text{em}} = 640$  nm,  $\lambda_{\text{ex}} = 560$ ).

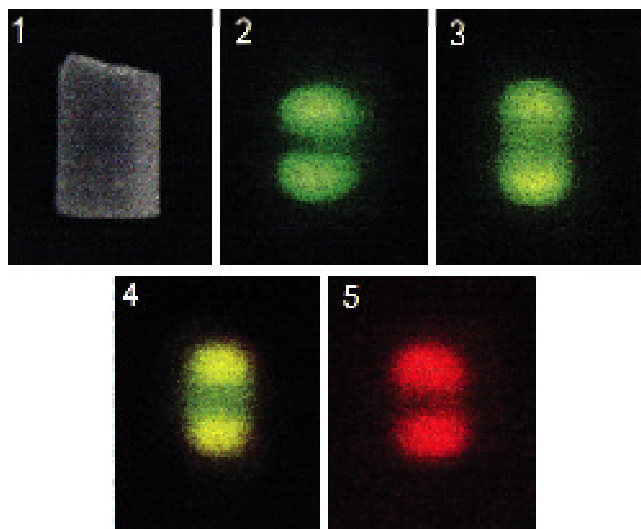


**Figure 4.** (1) Electron microscopy picture of a zeolite L crystal with a length of about  $1.5 \mu\text{m}$ . (2–5) True color fluorescence microscopy pictures of dye-loaded zeolite L crystals. (2–4) Fluorescence after excitation of only  $\text{Py}^+$ : (2) After 5 min exchange with  $\text{Py}^+$ , (3) after 2 h exchange with  $\text{Py}^+$ , and (4) after additional 2 h exchange with  $\text{Ox}^+$ . (5) The same as (4) but after specific excitation of only  $\text{Ox}^+$ .<sup>20</sup>

red  $\text{Ox}^+$  fluorescence.  $\text{Ox}^+$  was not excited directly, but via energy transfer from excited  $\text{Py}^+$  molecules. After specific excitation of  $\text{Ox}^+$  at 545–580 nm, picture 5, only the red fluorescence at both ends is visible while the middle part of the zeolite L crystal remains dark. This demonstrates nicely that a stacking of  $\text{Py}^+$  in the middle and  $\text{Ox}^+$  at both ends of the cylinders is achieved. It also illustrates that the first inserted  $\text{Py}^+$  does not leave the zeolite upon exchange with  $\text{Ox}^+$  and that inside the channels the dyes do not glide past each other. This observation which we have reported for the first time in ref 20 was a key step in the invention of the artificial antenna systems for light collection and transport.<sup>1,14,21</sup>

On the basis of space-filling geometrical arguments, we assumed in first reports on this system that  $\text{Py}^+$  and  $\text{Ox}^+$  are aligned along the channel axes of zeolite L.<sup>20,22</sup> More detailed investigations on better material and with more sophisticated techniques lead to the conclusion that  $\text{Py}^+$  and  $\text{Ox}^+$  belong to the type (ii) molecules for which the situation is more complicated,<sup>1,2</sup> as indicated by the following results. The luminescence of about  $2 \mu\text{m}$  long crystals, loaded with  $\text{Py}^+$  in

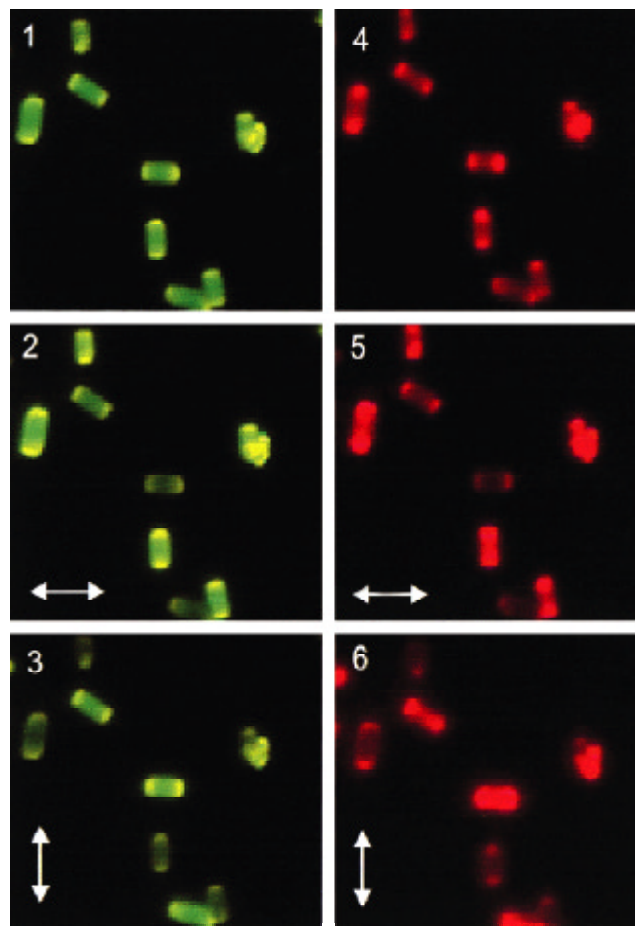


**Figure 5.** True color fluorescence microscopic pictures of  $\text{Py}^+$ -loaded and  $\text{Ox}^+$ -modified zeolite L crystals of about  $2 \mu\text{m}$  length. All pictures show the same crystals. (1–3) Excitation at 470–490 nm. (4–6) Excitation at 545–580 nm. (1) and (4) show fluorescence excited with nonpolarized light while the other pictures show fluorescence after excitation with linearly polarized light and nonpolarized observation. The arrows indicate the polarization direction of the excitation.

the middle region and a few  $\text{Ox}^+$  at both ends, upon linearly polarized excitation and non polarized observation, is illustrated in Figure 5. The difference between the three pictures 1–3 and 4–6 are the filters used for the excitation and for the observation of the emission. 1 shows the green fluorescence of  $\text{Py}^+$  after

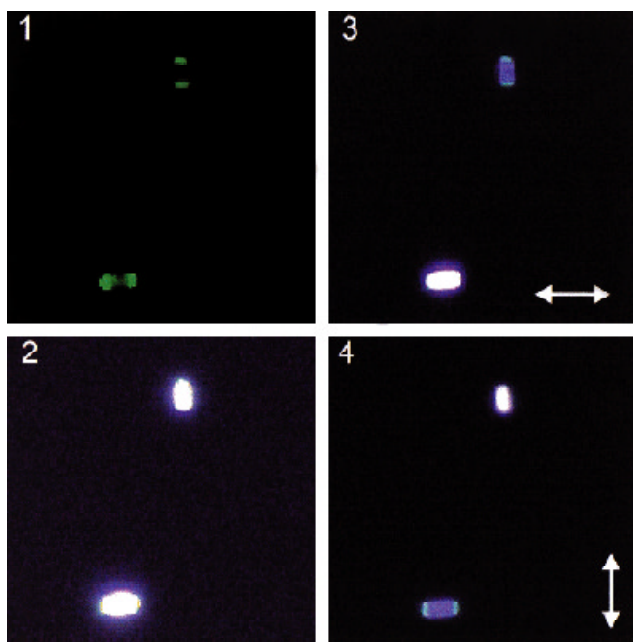


**Figure 6.** True color microscopy pictures of  $\text{Py}^+$ ,POPOP-zeolite L made on crystals of about  $2 \mu\text{m}$  length. (1) Specific excitation of  $\text{Py}^+$  at 470–490 nm. (2) Excitation at 330–385 nm. (3 and 4) show the same as (2) but after observation with a polarizer the direction of which is indicated by the arrows.

unpolarized excitation at 470–490 nm. The ends of the crystals appear yellow for the same reason as explained for picture 4 of Figure 4. The  $\text{Py}^+$  fluorescence after excitation with parallel polarized light ( $\leftrightarrow$ ) is seen in 2. ( $\leftrightarrow$ ) means that the excitation was polarized parallel to the bottom edge of the pictures and (vertical arrow) means perpendicular to it. Zeolite L crystals perpendicular to the polarization of the exciting light ( $\leftrightarrow$ ) show intense fluorescence, while those crystals parallel to it show only weak emission. After excitation with perpendicularly polarized light (vertical arrow) the reverse is observed, picture 3. The green and the yellow emission show the same behavior. This means that excited  $\text{Py}^+$  and  $\text{Ox}^+$  emit light with approximately the same polarization. This is further supported by the  $\text{Ox}^+$  fluorescence after specific excitation at 545–580 nm, as illustrated in 4–6. Similar observations are made when the crystals are excited with nonpolarized light upon polarized observation.

We expect that POPOP should belong to the type (iii) molecules, because it is significantly longer than two unit cells of zeolite L, as illustrated in Figure 2. The results reported in Figure 6, obtained on zeolite L crystals of about  $2 \mu\text{m}$  length, do support this. We show the luminescent behavior of two selected crystals, which were filled in the middle part by POPOP, and at both ends with a thin layer of  $\text{Py}^+$ . The latter is visible in picture 1, where  $\text{Py}^+$  is excited selectively at 470–490 nm. The characteristic green fluorescence of the  $\text{Py}^+$  located at both ends of the crystals is observed. The three other pictures show mainly the luminescence of POPOP: (2) Excitation at 330–385 nm; the POPOP fluorescence is strong, because of its much larger concentration, so that the green  $\text{Py}^+$  emission cannot be distinguished. (3 and 4) The same as 2 but observed by means of a polarizer, the direction of which is indicated in the same manner as in Figure 5. The result is obvious: strong POPOP emission in direction of the  $c$ -axis, weak emission perpendicular to it. The weak emission at both ends of the crystals in pictures 3 (upper) and 4 (lower) are due to the  $\text{Py}^+$  emission, which is approximately perpendicular to that of the

POPOP. Its appearance is due to energy transfer from excited POPOP and also to some direct absorption of light by  $\text{Py}^+$ .

#### 4. Imaging of Single $\text{Ox}^+$ -Loaded Zeolite L Crystals

The intensity of the light emitted from single crystallites was measured by means of a confocal laser scanning microscope in dependence upon the alignment of an analyzer, in order to quantitatively determine the polarization of the fluorescence from  $\text{Ox}^+$ -loaded zeolite L crystals. The zeolites with an  $\text{Ox}^+$  loading of  $p_{\text{Ox}} = 0.0006$  were found to be arbitrarily oriented on a glass surface. They were excited using 532 nm laser light. In step 1, the excitation light was circularly polarized, and in step 2, linearly polarized in two mutually perpendicular polarization directions. The intensity of the fluorescence was detected using an avalanche photodiode. A rotatable analyzer whose alignment can be adjusted from  $0^\circ$  to  $180^\circ$  in  $10^\circ$  steps was placed in the optical detection path.

A qualitative overview of the fluorescence anisotropy of single crystallites can be obtained by a false color image, which shows the polarization direction and the intensity at the three different excitation polarizations. The two linear excitation polarizations are chosen such that they lie parallel and perpendicular to the fluorescence image baseline. They are indicated by red and green arrows in Figure 7. The colors in the final image result by adding up the colors used to represent the fluorescence intensity at an analyzer setting of  $0^\circ$  (red) and the corresponding image using an analyzer setting of  $90^\circ$  (green). Note: The colors do not reflect the wavelengths of the emitted light.

A scanning electron micrograph is added to correlate the orientation of the zeolites and the polarization behavior. Crystallites whose length axis is oriented perpendicular to the baseline appear red, as in crystal 1. This means that the polarization direction in which the maximum fluorescence intensity is emitted lies parallel to the baseline and consequently perpendicular to the crystal axis. Green-colored zeolites are oriented parallel to the baseline and emit light that is predominantly perpendicularly polarized. Crystallites that are oriented parallel to one of the image diagonals are represented in yellow, as with crystal 2. Thus, the maximum fluorescence intensity lies at a polarization direction of roughly either  $45^\circ$  or  $135^\circ$ . These two scenarios cannot be differentiated in this experiment. Moreover, there are single zeolites, such as crystal 3, which stand on one of the two hexagonal endfaces. They appear circular in the optical images and emit intense fluorescence. Since their fluorescence intensity is the same regardless of whether the analyzer is set at  $0^\circ$  or  $90^\circ$ , they likewise appear yellow in the image.

When comparing the fluorescence images obtained from the two linear excitation polarizations with the fluorescence image of the circular excitation, it is noticeable that the color values depicting the single crystallites remain the same, whereas the intensities vary considerably. Due to the fact that the colors symbolize the polarization direction in which the maximum fluorescence intensity is emitted, it is obvious that the polarization of the fluorescence does not vary during the different excitations. Crystallites that are depicted red fluoresce most strongly at a parallel excitation and weakly at a perpendicular excitation. It is exactly the inverse for crystallites depicted green. The intensity of circular excitation lies somewhere between the values for the two linear excitations. Crystallites that are depicted yellow appear in all three images with nearly the same intensity. Crystal 2 fluoresces at perpendicular excitation somewhat stronger than at parallel excitation. This indicates that the angle between the baseline and the crystal axis of crystal 2 is somewhat smaller than  $45^\circ$ , which can also be seen on the

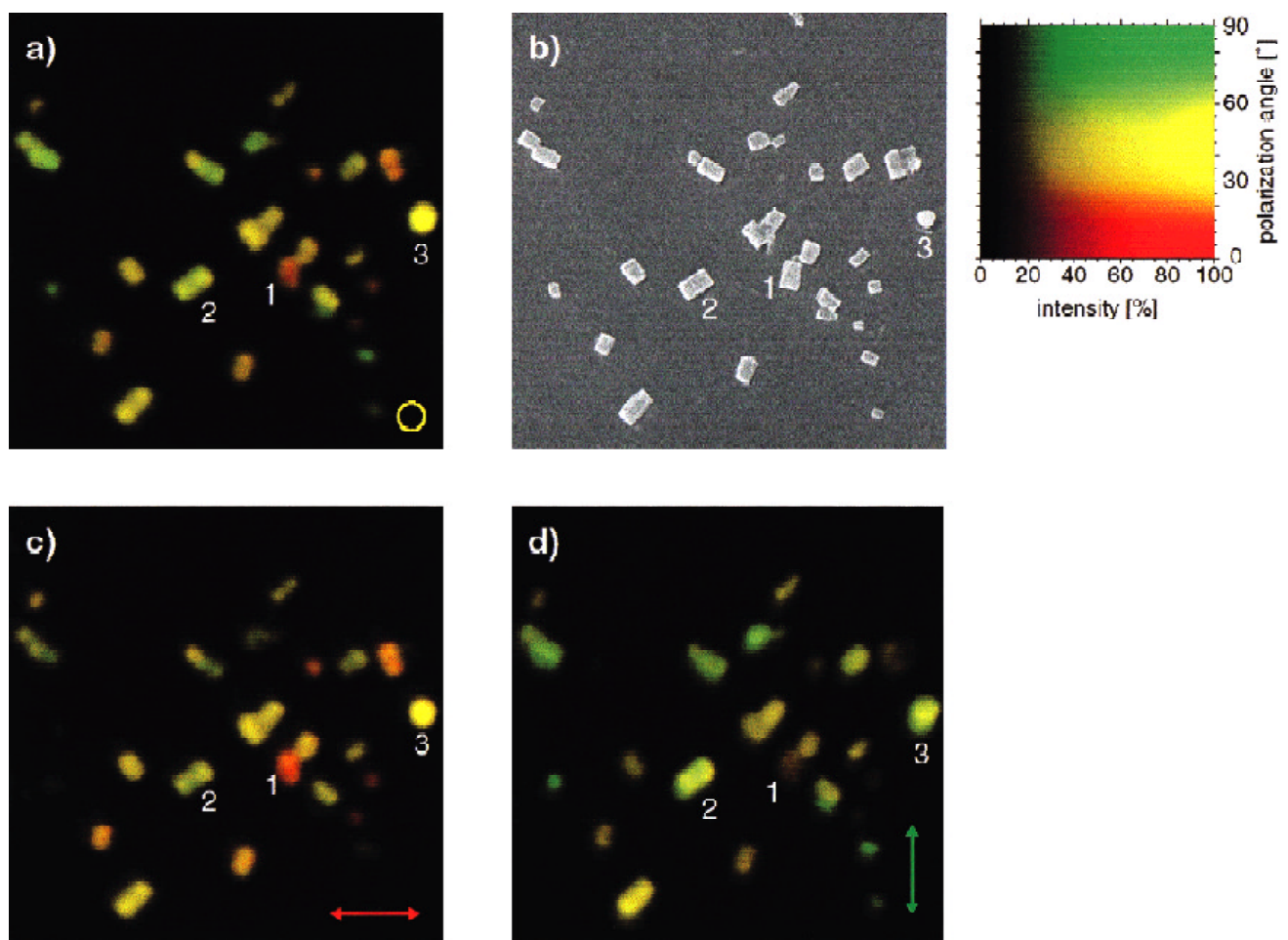


**Figure 7.** (a,c,d) False color images which show the polarization and intensity of the fluorescence of  $\text{Ox}^+$ -loaded zeolite L crystals for linearly polarized excitation in the direction of the arrow and for circularly polarized excitation (circle). (b) Scanning electron micrograph of the sample. The image colors do not correspond to the wavelength of the fluorescence light. Rather, they correlate to the polarization direction in which the maximum fluorescence is emitted (see color table at the right side).

electron micrograph. Crystal 3 presents an exception to the fluorescence behavior described before. The intensity of the emitted light appears to be nearly the same for all three excitation polarizations. However, the color for parallel excitation is slightly shifted toward red, whereas at perpendicular excitation it is shifted toward green. Thus, a polarization appears that is not observed by circular excitation.

A more precise description results from a detailed polarization analysis of the fluorescence of single crystallites. In Figure 8 (upper row), the measured fluorescence intensities of the representative crystals 1, 2, and 3 are portrayed in dependence upon the analyzer setting at the three different excitation polarizations. The lying crystals 1 and 2 show intensity maxima and minima at all types of excitation.

The data shows that crystals, which lie nearly parallel to one of the two linear excitation directions, such as crystal 1, have comparable traces at circular and linear excitations. In these cases the maxima and minima of the three curves lie at roughly the same analyzer setting, but, the intensities differ substantially. At linear excitation perpendicular to the crystal axis, i.e., for crystal 1 parallel to the baseline of the image, the maximum fluorescence intensity is approximately a factor of 4 larger than that at linear excitation in the direction of the crystal axis. For crystal 2, which is oriented at an angle of about  $30^\circ$  to the baseline, the maximum intensities of the two linear excitation polarizations differ only by a factor of 2. In contrast to crystal 1, the maxima and minima for linear excitation are no longer

found at the same analyzer angle, as with circular excitation. Rather, they are shifted by approximately  $+10^\circ$  and  $-10^\circ$ . For both lying crystals, the intensity at circular excitation corresponds to an average of the intensities at the two perpendicular linear excitations. The polarization directions in which the maximum fluorescence is emitted at circular excitation lie in both cases exactly perpendicular to the crystal axis. For the standing crystal 3, the intensity traces for the different excitation polarizations show a completely different behavior. The intensity at circular excitation is for the most part constant. Thus, the fluorescence is most likely completely unpolarized. Furthermore, for linearly polarized excitation the maximum fluorescence intensity is emitted parallel to the excitation direction in each case.

The goal of the following considerations is to find an orientation distribution, which can be fitted consistently to all polarization data in this section. Such a global polarization analysis leaves not much room for various possible orientation distributions. Arguments if and how the dye molecules can indeed assume the proposed orientations in the zeolite L cavities are left to section 7. The experimental data obtained from crystals standing on one of their hexagonal endfaces, such as crystal 3, suggest that the transition moments of the dye molecules are fanned out in a radial fashion perpendicular to the crystal axis. Furthermore, the 6-fold symmetry of the crystal endface leads us to assume also 6-fold symmetry in the radial distribution. Considering the lying crystals, as for example 1 and 2, we note that the radial distribution around the crystal

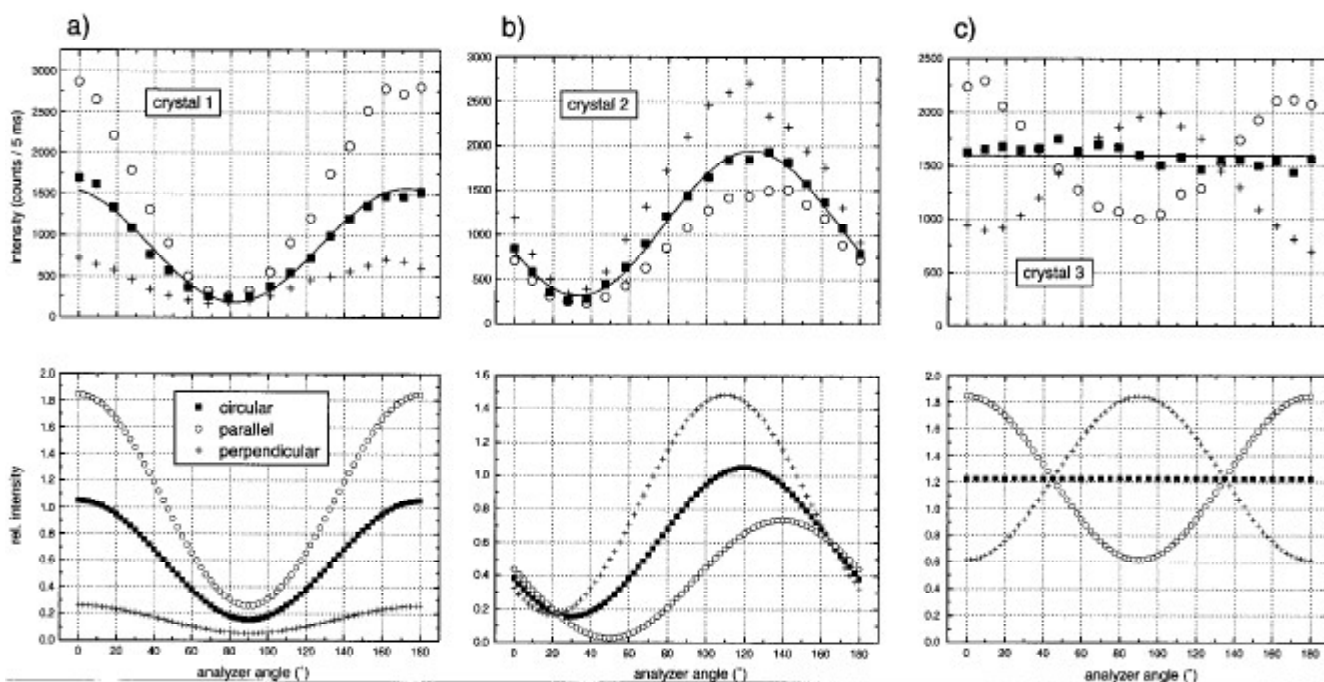


**Figure 8.** (Upper) Measured fluorescence for crystals 1, 2 and 3 at circularly and linearly polarized excitation, dependent upon the analyzer transmission direction. The solid lines show the intensity function (eq 1) for circular excitation fitted to the experimental data. (Lower) Intensity functions calculated using a half-cone angle of  $\alpha = 72^\circ$  (see Figure 9) at circular and linear excitation for crystals 1, 2, and 3.

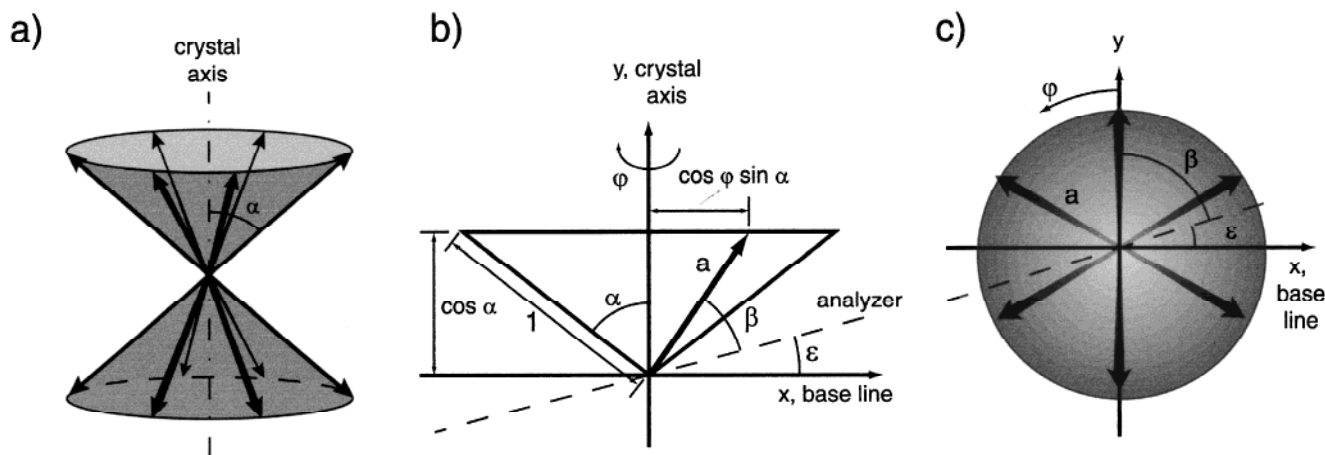


**Figure 9.** Schematic representation of the six possible orientations of the molecules' transition dipole moment on the surface of a double cone and parameters for calculation: (a, b) for a lying crystal, (c) for a standing crystal.

axis must form a double cone with a rather large opening half-angle  $\alpha$  with respect to the crystal axis (see Figure 9) in order to generate the large polarization component perpendicular to the crystal axis. If we would only consider the data from the standing crystals there could in principle also exist other orientation distributions. However, we found no other scenario, which can be fitted reasonably at the same time to all data.

Assuming the distribution of the transition moments proposed above, the relative fluorescence intensities for lying and standing crystallites for different excitation polarizations can be calculated. For the system depicted, the model assumes that a plane wave in the direction of the optical axis of the system is used to illuminate the zeolites and that the fluorescence is detected likewise in the direction of the optical axis. Furthermore, the influence of the background signal due to impurities as well as the birefringence of the zeolites is not included in the calculation. These influences are negligible with respect to the uncertainties of the measurement. The background signal is unpolarized only for circular excitation; for linear excitation, the polarization of

the background signal is in the direction of polarization of the exciting light. Using this, the relative fluorescence intensities can be obtained by adding the intensities emitted by  $\text{Ox}^+$  molecules with transition moments in the six possible orientations.

The parameters used to calculate an equation for the fluorescence intensity of a lying crystal are pictured in Figure 9b, in which the projection of one-half of the double cone with a half-cone angle of  $\alpha$  is shown. The arrow of the length  $a$  symbolizes one possible orientation of the transition moment on the surface of the double cone. The orientation of the analyzer with respect to the baseline  $x$  is measured by the angle  $\epsilon$ . In order to keep the calculation simple at this moment, we consider a situation where the crystal axis is oriented perpendicular to the baseline. The value of  $a$  is proportional to the length of the projection of the transition moment into the  $x,y$ -plane. The angle  $\varphi$  describes the rotation around the crystal axis, and  $\beta$  symbolizes the angle between analyzer and transition moment orientation. If the molecule is excited with circularly polarized light

in the  $x,y$ -plane the excitation rate is proportional to  $|a|^2$ , likewise the fluorescence rate detected along the analyzer axis is  $|a|^2 \cos^2 \beta$ . Taking excitation and emission together, the fluorescence rate for this particular geometry is proportional to  $|a|^4 \cos^2 \beta$ . The overall intensity of one crystal results from summing up the emitted intensities of molecules with transition moments at all six possible orientations:

$$I_{\text{rel}} = \sum_{i=1}^6 |a_i|^4 \cos^2 \beta_i$$

$$= \sum_{i=1}^6 [(\cos \varphi_i \sin \alpha)^2 + \cos^2 \alpha]^2$$

$$\sin^2(\epsilon + \arctan(\cos \varphi_i \tan \alpha)) \quad (1)$$

The possible values of  $\varphi_i$  are  $0^\circ$ ,  $60^\circ$ ,  $120^\circ$ ,  $180^\circ$ ,  $240^\circ$ , and  $300^\circ$  (see Figure 9c). With this, the previous equation results in

$$I_{\text{rel}} = \sin^2(\epsilon + \alpha) + \sin^2(\epsilon - \alpha) + (1/8 \sin^4 \alpha - 3 \sin^2 \alpha + 2(\sin^2(\epsilon + \arctan(1/2 \tan \alpha)) + \sin^2(\epsilon - \arctan(1/2 \tan \alpha))) \quad (2)$$

Equation 2 is only valid for crystals whose axis is oriented perpendicular to the baseline. For all other cases an additional phase shift  $\delta$  has to be added to the angle  $\epsilon$  between the baseline and the analyzer, whereby  $90^\circ - \delta$  characterizes the angle between crystal axis and baseline.

In the case of standing crystals one has to choose a view along the crystal axis. With the above-described parameters, the relative fluorescence intensity can be calculated in a similar way. The result no longer depends on the analyzer orientation  $\epsilon$ :

$$I_{\text{rel}} = 3/2 \sin^4 \alpha \quad (3)$$

The relative intensities for linearly polarized excitation can be found using analogous calculations. For details see Appendix.

The fit of eq 2 to the experimental data of 27 lying crystallites at circular excitation (see Figure 8, a and b, above), yields a half-opening angle  $\alpha$  of  $72^\circ \pm 3^\circ$ . Furthermore, the fit results in a phase shift of the function, which is reflected in the angle between the image baseline and the crystal axis. It also results in a factor for the absolute intensity, which correlates very well with the size of the individual crystals. By calculating the intensity for lying and standing zeolites at circularly and linearly polarized excitation with the value obtained for  $\alpha$ , the experimental data of crystals 1, 2, and 3 can be compared with the theoretical results of the model. The calculated course of the function as well as the intensity behavior for the various excitation polarizations is in good agreement with the measured values, as shown in Figure 8. However, the intensity differences for the minima of the lying crystals 1 and 2 in the three measurement curves are not as large as model calculations predict. This deviation can be explained by taking the polarization of the background signal at linear excitations into account. Furthermore, for crystal 2 one can see that the measured orientations of the maxima and minima at circularly and linearly polarized excitations are not as strongly shifted toward each other as in the model's calculations. This effect is most likely due to the fact that the background signal was not considered. If a constant background signal at circular excitation is subtracted from the measured data, the relation between the maximum and minimum intensity increases. This causes the

opening angle  $\alpha$  of the cone to increase by several degrees. Hence, the positions of the calculated maxima and minima of crystals which are not parallel to one of the two linear excitation directions do converge.

## 5. Geometrical Reasoning and Molecular Orbital Calculations

The length of POPOP in  $x$ -direction is about 19 Å (see Figure 2). To obtain the van der Waals length, about 2 Å have to be added. Its length then corresponds to the length of nearly three zeolite L unit cells. The height of the flat molecule is about 6.2 Å. Adding 2 Å to obtain the van der Waals height raises the question if POPOP might be too large to enter the 12-membered ring window. We found that the kinetic diameter of POPOP allows it to enter the channels of zeolite L at elevated temperature where it has no other choice but to align along the  $c$ -axis. The first electronic transition of POPOP is of  $\pi, \pi^*$  type and polarized along the  $x$ -axis. This means that the observations reported in Figure 6 clearly support the space-filling geometrical arguments according to which POPOP does align along the  $c$ -axis in zeolite L. The situation is more complex for  $\text{Ox}^+$  and  $\text{Py}^+$ . Their length is 11.3 Å. Adding 2 Å to obtain the van der Waals length gives 13.3 Å. On the basis of the data reported in the previous sections we must revise our earlier assumption that these dyes do align along the  $c$ -axis of zeolite L. To understand the experimental data we first study the different positions of these dyes in the main channels. We then also investigate the nature of the first electronic transitions in more detail. We distinguish four degrees of freedom: translation along the  $c$ -axis, rotation around the channel axes  $\beta$ , rotation around the molecules axes  $\gamma$ , and tilting  $\alpha$ . Detailed investigations showed that it is sufficient to consider the two positions along the  $c$ -axis shown in Figure 10 (top) and we found that the determining angle is  $\alpha$ .

What are acceptable  $\alpha$ -values? We discuss this question by means of geometrical arguments because energy minimization procedures are, unfortunately, not to be trusted for this system, even when using advanced computational procedures. Situations for atom-atom distances always larger than the van der Waals radii from ref 23 have been investigated. Exceptions are the  $\text{C}_{\text{dye}}\text{H}\cdots\text{O}_{\text{zeolite}}$  distances that turned out to be of special importance and which have been varied. We show them for  $\text{Py}^+$  and  $\text{Ox}^+$  in Figure 10 (left) as a function of  $\alpha$ . The shortest  $\text{CH}\cdots\text{O}_{\text{zeolite}}$  distance found in the literature is shown as horizontal line.<sup>24</sup>  $\text{Py}^+$  shows shorter  $\text{C}_{\text{dye}}\text{H}\cdots\text{O}_{\text{zeolite}}$  distances than  $\text{Ox}^+$ . This is due to the CH group which replaces the aromatic nitrogen atom in  $\text{Ox}^+$  and which makes a short contact in the 12-ring of the zeolite. Based on this, the smallest acceptable  $\text{C}_{\text{dye}}\text{H}\cdots\text{O}_{\text{zeolite}}$  distances lead to a largest acceptable angle  $\alpha$  of about  $40^\circ$  for  $\text{Ox}^+$  and  $30^\circ$  for  $\text{Py}^+$ . These angles can only be realized for the position on the  $c$ -axis shown on the left side of Figure 10. This result seems to confirm our previously reported reasoning that  $\text{Py}^+$  and  $\text{Ox}^+$  basically align along the  $c$ -axis. However, the experimental results communicated in sections 3 and 4 do not. We have therefore investigated an additional possibility illustrated on the right side of Figure 10. We found that  $\text{Ox}^+$  and  $\text{Py}^+$  have indeed a chance to lie perpendicular to the  $c$ -axis, from a geometrical space-filling point of view. The  $\text{H}_2\text{N}_{\text{dye}}\cdots\text{O}_{\text{zeolite}}$  and  $\text{N}_{\text{dye}}\text{H}_2\cdots\text{O}_{\text{zeolite}}$  distances are 3.3 and 2.5 Å, respectively, which is reasonable. In Figure 10 the shortest contact distances for this position are reported as a function of  $\alpha$ . The critical  $\text{H}_2\text{N}_{\text{dye}}\cdots\text{O}_{\text{zeolite}}$  distance is about 3.1 Å only within an angle of about  $90^\circ$ . Deviations of this angle rapidly result in hardly acceptable situations. When

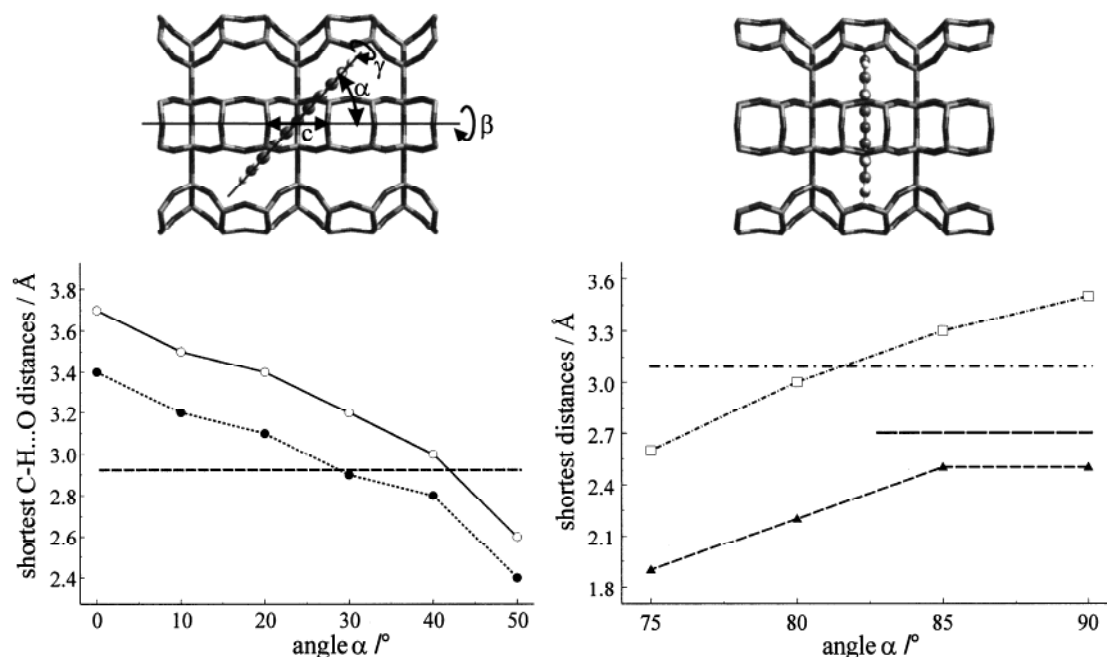


**Figure 10.** Positions of  $Ox^+$  and  $Py^+$  in the main channel of zeolite L. (Top, left) Degrees of freedom of a planar dye molecule in the cavities of zeolite L. (Bottom, left) Shortest  $C_{dye}-H\cdots O_{zeolite}$  distances of  $Py^+$  (dotted) and  $Ox^+$  (solid) when the molecule is rotated around  $\alpha$  and centered in the middle of the 12 ring. (Top, right)  $Ox^+$  lying across the channel of zeolite L. (Bottom, right) Shortest distances of  $Py^+$  and  $Ox^+$  when the molecule is rotated around  $\alpha$  and centered in the middle of the unit cell;  $H_2N_{dye}\cdots O_{zeolite}$  (dash-dot) and  $N_{dye}H_2\cdots O_{zeolite}$  (dashed). Summed up van der Waals radii are indicated by horizontal lines.

$\alpha$  is  $75^\circ$  then the  $H_2N_{dye}\cdots O_{zeolite}$  distance is  $2.6 \text{ \AA}$  and therefore far beyond the summed up van der Waals radius indicated by the dashed horizontal line. The behavior of  $Py^+$  and  $Ox^+$  is the same, because the terminal  $NH_2$  groups control the critical distances. We conclude that geometrical arguments give room for only two probable arrangements of  $Py^+$  and  $Ox^+$ : an angle  $\alpha$  of up to  $40^\circ$  for  $Ox^+$  and up to  $30^\circ$  for  $Py^+$ , and an angle  $\alpha$  of about  $90^\circ$  for both of them. Because of the severely limited space we cannot answer the question how the molecules could possibly find their way into the  $90^\circ$  position, despite the fact that kinetic radii can be unexpectedly large as we observed for POPOP and as reported for other systems.<sup>25</sup>

Although the main features of the electronic structure of dyes with similar structures as  $Py^+$  and  $Ox^+$  are well-known,<sup>26</sup> it is necessary to consider them in more detail. We are especially interested in the symmetry of the first electronic transitions. The frontier orbital region of  $Py^+$ , as obtained from an EHMO calculation, is illustrated in Figure 11. The HOMO/LUMO region consists of  $\pi$  orbitals of  $a_2$  and  $b_2$  symmetry. This leads to excited electronic configurations of  $a_1$  and  $b_1$  symmetry and to nonzero transition moments in  $z$ - and  $x$ -direction, respectively. The LUMO  $\leftarrow$  HOMO transition is  $x$ -polarized and bears large oscillator strength. It is closely followed by a much weaker  $z$ -polarized transition. Additional excited  $\pi,\pi^*$  configurations of  $a_1$  and of  $b_1$  symmetry can lead to configuration interaction, which must be considered. The main part of the HOMO is located at the terminal nitrogen atoms while the LUMO is concentrated in the middle of the molecule. The  $1n(a_1)$  orbital appears significantly below the HOMO-1. It gives rise to a very weak but allowed transition along the  $y$ -axis. The calculated oscillator strength is in the order of  $10^{-4}$ .

The PPP procedure has proven to be an excellent tool for studying the consequences of configuration interaction (CI) important in  $\pi,\pi^*$  transitions of aromatic molecules. The  $S_1$  state is only little altered by the CI treatment with 49 configurations, in contrast to the higher states. This means that the intense  $S_1 \leftarrow S_0$  absorption band can essentially be attributed to a  $1\pi^*(b_2)$

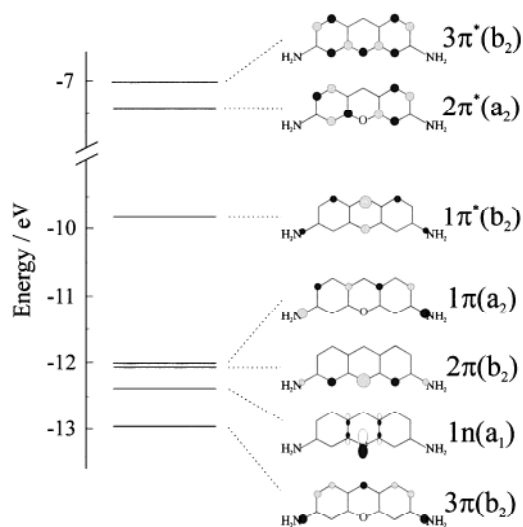


**Figure 11.** One-electron energy level diagram of  $Py^+$ .

$\leftarrow 1\pi(a_2)$  transition, as reported in earlier studies of similar dyes.<sup>27,28</sup> We observe a considerable energy splitting between the  $S_1$  and the  $S_2$  states. The oscillator strength of the  $S_1 \leftarrow S_0$  transition, oriented along the  $x$ -axis, is about 2 orders of magnitude larger than those of the  $z$ -polarized  $S_2 \leftarrow S_0$  and  $S_3 \leftarrow S_0$  transitions. Similar results have been obtained for  $Ox^+$ . A comparison of the experimental spectra of  $Py^+$  and  $Ox^+$  and the calculation is illustrated in Figure 12. The heights of the lines represent the calculated relative intensities.  $x$  and  $z$  indicate the polarization of the  $S_n \leftarrow S_0 \pi,\pi^*$  transitions. The two weak  $z$ -polarized  $S_3, S_2 \leftarrow S_0$  transitions, which appear in the specially indicated region, are well separated from the main absorption band. The higher energy bands we have calculated are not indicated because they are not relevant for this study. Also not indicated is the  $\pi^* \leftarrow n$  transition. Its position can be estimated to be above  $25\,000 \text{ cm}^{-1}$  for  $Py^+$  where only the oxygen atom is involved. The highest  $n$ -orbital in  $Ox^+$  is concentrated on

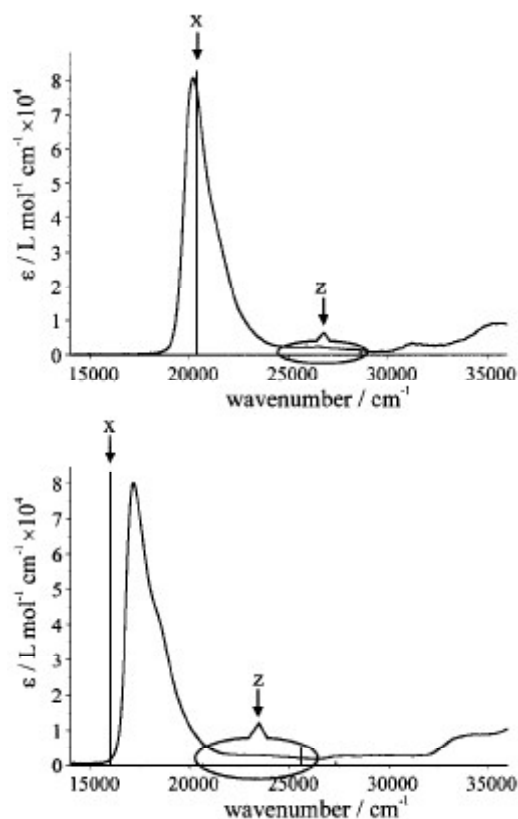


**Figure 12.** Experimental absorption spectrum of  $\text{Py}^+$  (upper) and  $\text{Ox}^+$  (lower) in water at room temperature and calculated electronic  $\pi, \pi^*$  transitions.

the nitrogen atom in the aromatic ring. It gives rise to a very weak  $y$ -polarized  $\pi^* \leftarrow n$  transition which we expect to be hidden somewhere on the high-energy side of the intense  $S_1 \leftarrow S_0$  absorption band because otherwise  $\text{Ox}^+$  would not show such intense fluorescence.  $\pi^* \leftarrow n$  transitions are known to shift considerably, depending on the solvent.<sup>29,30</sup> The important result for this study is that the  $z$ -polarized  $\pi, \pi^*$  transitions are weak and well separated from the  $S_1 \leftarrow S_0$  but nevertheless not at much higher energy.

## 6. Experimental Section

**Materials.** Zeolite L. The pure potassium form of zeolite L  $\text{K}_9(\text{AlO}_2)_9(\text{SiO}_2)_{27} \cdot 21\text{H}_2\text{O}$  was synthesized as described in refs 3 and 21.  $\text{Py}^+$  and  $\text{Ox}^+$  were synthesized as reported in ref 21. 5,5'-Diphenyl-2,2'-*p*-phenylenebis(oxazole) (POPOP) from Fluka ( $\sim 99\%$ ) was used as received.

**Dye-Loaded Zeolite Materials.**  $\text{Py}^+$ -loaded and  $\text{Ox}^+$ -modified zeolite L crystals were prepared as described in refs 3 and 21. The loading of the samples in Figure 5 was  $p_{\text{py}} = 0.11$  with about 4  $\text{Ox}^+$  per channel. That of the crystals reported in Figures 7 and 8 was  $p_{\text{ox}} = 0.0006$ . Aggregates were removed from the surface of the crystals as described in ref 3. The preparation of the  $\text{Py}^+$ , POPOP-zeolite L material was performed by gas phase reaction of dehydrated zeolite L with POPOP at 250 °C followed by ion exchange with  $\text{Py}^+$  at 80 °C from an aqueous suspension. Experimental details for the preparation of similar samples are reported elsewhere.<sup>14</sup> The resulting material had a loading of 0.2 POPOP/u.c. ( $p_{\text{POPOP}} \approx 0.6$ ) and of about 4  $\text{Py}^+$  per channel.

**Physical Measurements.** UV/vis spectra were recorded on a Lambda 14 spectrophotometer (Perkin-Elmer). Fluorescence spectra were recorded on a luminescence spectrometer LS 50B (Perkin-Elmer). Optical microscopy pictures of fluorescent

samples were taken with 1000 times enlargement on an Olympus BX 60 microscope provided with a Kappa CF 20 DCX Air K2 CCD camera. The light stemming from a 100 W halogen or mercury lamp was passed through appropriate excitation cubes composed of a narrow band excitation filter, a dichroic mirror, and a cutoff barrier filter. For the observation of the POPOP,  $\text{Py}^+$ , and  $\text{Ox}^+$  fluorescence the appropriate cubes were selected to excite the investigated molecules in the region of the first  $\pi, \pi^*$  absorption band (see Figure 3): U-MWU (330–385 nm), U-MNB (470–490 nm), and U-MWIY (545–580 nm). A polarization filter was used either in the excitation or in the analyzer light beam. Images were recorded with Kappa Image-Base software.

**Single-Crystal Imaging.** A high-resolution scanning confocal microscope was used to image the fluorescence of single dye-loaded crystals. The sample was prepared by pushing a freshly cleaved glass fiber into an aqueous suspension of dye-loaded zeolite microcrystals. Several crystals adhered and were found to be randomly distributed on the glass surface after the water had evaporated. The molecules were excited by a Nd:YVO<sub>4</sub> laser ( $\lambda = 532$  nm), and the polarization of the excitation beam was controlled by half and quarter waveplates to achieve circularly or linearly polarized light in the desired direction. A Zeiss 100 $\times$ , NA 0.75 objective lens was used for focusing the excitation light and for collecting the fluorescence. The excitation light reflected from the sample was suppressed 6 orders of magnitude by a holographic notch filter (Kaiser). The remaining fluorescence beam passed through a broadband analyzer. For detection, the beam was focused onto an avalanche photodiode (EG&G, SPCM 200). Images were recorded by scanning the sample in a raster-like fashion and collecting the data point by point. Details of the setup are described in refs 31 and 32. The polarization direction of the fluorescence light was selected by rotating the analyzer before an image was taken. To evaluate the fluorescence intensity of single crystals in dependence of the polarization, the values of five pixels at the most intense location of each crystal were selected and averaged.

**Force Field and Molecular Orbital Calculations.** *Force Field.* Geometrical aspects and optimization of the dye structures were performed by the program CERIU2. The optimization was done with the implemented MMFFs method.<sup>33</sup> The zeolite structure was taken from powder X-ray data.<sup>11</sup> Critical distances were found by close contact monitoring.

*Molecular Orbitals.* Molecular orbitals were investigated by means of the EHMO (extended Hückel molecular orbitals)<sup>34</sup> method using ICONC-EDiT.<sup>30,35</sup> Off-diagonal elements were calculated by the weighted Wolfsberg–Helmholz<sup>36</sup> formula with a distance dependent Hückel constant.<sup>37</sup> Standard parameters as given in ref 35 were used.

*Configuration Interaction (CI).* The PPP (Pariser, Parr, Pople) method was used to calculate the  $S_n$  singlet states.<sup>38</sup> Forty-nine ( $\pi, \pi^*$ ) configurations were included in the CI calculations. The parameters reported in ref 39 were used with the exception of the  $\text{NH}_2$  groups for which  $U_{\text{NH}_2} = -24.22$  eV,  $\gamma_{\text{NH}_2} = 18$  eV, and  $\beta_{\text{NH}_2, X} = -2.09$  eV was applied.

## 7. Discussion and Conclusions

Fluorescence microscopy, single-crystal imaging, and space-filling arguments led to new information about the orientation of dye molecules inside the nano channels of zeolite L. Observations made on POPOP, the length of which corresponds to nearly three unit cells of zeolite L in the  $c$ -direction, and the fact that the transition dipole moment is oriented parallel to the molecule's long axis, unambiguously lead to the result that this

dye is aligned along the channel axis. The POPOP-loaded crystals, illustrated in Figure 6, were modified at their ends with  $\text{Py}^+$ . We observed that maximum polarization of the green  $\text{Py}^+$  luminescence appears nearly perpendicular to that of the POPOP, which was surprising. Fluorescence microscopy pictures of  $\text{Py}^+$ -loaded zeolite L crystals, modified at their ends with  $\text{Ox}^+$  showed that the orientation of the  $S_1 \leftarrow S_0$  transition moment of  $\text{Py}^+$  and  $\text{Ox}^+$  in the zeolite is approximately the same.

Quantitative measurements of the fluorescence polarization were therefore performed with single  $\text{Ox}^+$ -loaded zeolite L crystals. The result is that a cone-shaped orientation distribution of the transition dipole moments with a half opening angle of  $72^\circ \pm 3^\circ$  around the crystal axis must be assumed to describe consistently all the polarization data. According to the crystal structure model, however, the maximum possible cone half-angles for  $\text{Py}^+$  and  $\text{Ox}^+$  are  $30^\circ$  and  $40^\circ$ , respectively. An explanation of the discrepancy between the orientation of the transition dipole moments obtained from the optical measurements and the orientation of the molecular axis by an optical transition polarized perpendicular to the long molecule axis is in contradiction with our experimental and theoretical findings. The possibility of an orientation distribution where a large fraction of the guest molecules would be oriented perpendicular to the channels is excluded by the experimental data reported in section 4. Let us consider for example a crystal with such an orientation distribution which is excited along the long axis such as crystal 1 in Figure 7. What we would expect to observe is a local intensity maximum when the analyzer setting is along the crystal axis. This is obviously not the case, as can be seen in Figure 8. The same is valid for a cone-shaped distribution of the two populations with the maximum allowed half-cone angles.

The extraframework cations protrude into the void internal space of zeolites and expose adsorbed guest molecules to considerable electrical fields.<sup>40</sup> As a result, otherwise inactive molecules like  $\text{H}_2$ ,  $\text{N}_2$ , and  $\text{O}_2$  are polarized and show IR spectra when embedded in a zeolite.<sup>41–43</sup> Stark-effect experiments performed with spectral hole-burning spectroscopy on oxazine 4, which is  $\text{Ox}^+$  substituted with methyl groups at the 2 and 7 positions and ethyl groups at the endstanding nitrogens, show a large matrix-induced dipole moment.<sup>44</sup> An explanation consistent with all the facts is that  $\text{Ox}^+$  is oriented in a cone of about  $40^\circ$  opening with respect to the  $c$ -axis so that it is exposed to a considerable anisotropic electrical field. This induces a mixing of the first  $x$ - and the  $z$ -polarized electronic transitions with the consequence that the effective transition moment of the molecule is turned away from the long axis. The observed polarization angle of  $72^\circ$  would then be the sum of the molecules tilting angle and the turning of the transition moment by Stark effect. Similar arguments apply for the  $\text{Py}^+$  for which, however, only qualitative observations are available so far.<sup>2</sup>

In summary, we have shown that it is not trivial to predict the fluorescence polarization of dye-loaded zeolite crystals from structural data, nor can the orientation of the dye molecules directly be predicted from the optical data. Electric field strength in zeolites of several MV/cm up to GV/cm have been reported in the literature.<sup>40–43</sup> Further knowledge of its influence on the electronic properties of dye molecules is desirable. This is obtained from detailed optical measurements performed with single microcrystals in combination with mathematical modeling. They lead to a consistent picture about transition moment

distribution of the guest molecules and, hence, reveal details which would be lost in an ensemble measurement due to spatial averaging.

**Acknowledgment.** This work was supported by the Swiss National Science Foundation Project NFP 4047-057481 and by the Project NF 2000-0534 14/98/1. We would like to thank Dr. A. Currao for helpful discussions and Dr. V. Sklover for his support with the Cerius program.

### Appendix: Derivation of the Equations for Linearly Polarized Excitation

The parameters used to calculate the fluorescence intensity of lying crystals at linearly polarized excitation are pictured in Figure 13. At linear excitation the fluorescence intensity not only depends on the orientation of the transition moments on the double cone but also on the angle between the transition moment's direction and the polarization of the exciting light. Therefore, in addition to the parameters pictured in Figure 9b, the two angles  $\alpha'$  and  $\gamma$  are introduced.  $\alpha'$  describes the angle between the  $y$ -axis and the projection of the transition moment into the  $x,y$ -plane of length  $a$ , and  $\gamma$  characterizes the angle between the  $y$ -direction and the crystal axis of the zeolite and corresponds with the orientation of the crystallite on the sample.

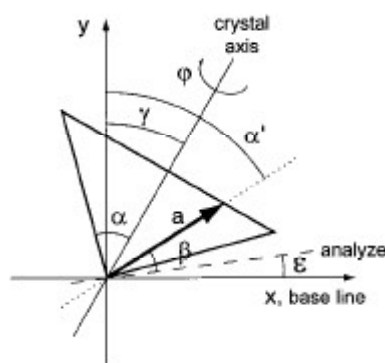


**Figure 13.** Sketch of transition moments and parameters for calculating the fluorescence intensity at linearly polarized excitation.

The angle  $\alpha'$  can be expressed in dependence on  $\varphi$ ,  $\alpha$ , and  $\gamma$  as follows:

$$\alpha' = \arctan(\cos \varphi \tan \alpha) + \gamma \quad (\text{A.1})$$

The angle  $\beta$  between transition moment and analyzer setting  $\epsilon$  can be calculated by

$$\beta = \epsilon + \alpha' - 90^\circ = \epsilon + \arctan(\cos \varphi \tan \alpha) + \gamma - 90^\circ \quad (\text{A.2})$$

At linear excitation in the  $x$ -direction the emitted intensity of one dye molecule is not only proportional to  $a^4 \cos^2 \beta$  as given in eq 1 but also to  $\sin^2 \alpha'$ . Summing up the intensities from all possible orientations of the transition moment leads to

$$\begin{aligned} I_{\text{rel}}^x &= \sum_{i=1}^6 |\alpha_i|^4 \sin^2 \alpha_i' \cos^2 \beta_i \\ &= \sum_{i=1}^6 ((\cos \varphi_i \sin \alpha)^2 + \cos^2 \alpha)^2 \\ &\quad \sin^2(\arctan(\cos \varphi_i \tan \alpha) + \gamma) \sin^2(\epsilon + \gamma + \\ &\quad \arctan(\cos \varphi_i \tan \alpha)) \quad (\text{A.3}) \end{aligned}$$

Calculating eq A.3 with the allowed values for  $\varphi_i$  yields the

relative fluorescence intensity:

$$I_{\text{rel}}^x = \sin^2(\gamma + \alpha) \sin^2(\epsilon + \gamma + \alpha) + \sin^2(\gamma - \alpha) \sin^2(\epsilon + \gamma - \alpha) + \left(\frac{9}{8} \sin^4 \alpha - 3 \sin^2 \alpha + 2\right) [\sin^2(\gamma + \arctan(1/2 \tan \alpha)) \sin^2(\epsilon + \gamma + \arctan(1/2 \tan \alpha)) + \sin^2(\gamma - \arctan(1/2 \tan \alpha)) \sin^2(\epsilon + \gamma - \arctan(1/2 \tan \alpha))] \quad (\text{A.4})$$

At linear excitation in the  $y$ -direction the fluorescence rate of a single molecule is proportional to  $a^4 \cos^2 \beta \cos^2 \alpha'$ . The relative fluorescence intensity follows by an analogous calculation:

$$I_{\text{rel}}^y = \cos^2(\gamma + \alpha) \sin^2(\epsilon + \gamma + \alpha) + \cos^2(\gamma - \alpha) \sin^2(\epsilon + \gamma - \alpha) + \left(\frac{9}{8} \sin^4 \alpha - 3 \sin^2 \alpha + 2\right) [\cos^2(\gamma + \arctan(1/2 \tan \alpha)) \sin^2(\epsilon + \gamma + \arctan(1/2 \tan \alpha)) + \cos^2(\gamma - \arctan(1/2 \tan \alpha)) \sin^2(\epsilon + \gamma - \arctan(1/2 \tan \alpha))] \quad (\text{A.5})$$

The deviation of the relative fluorescence intensity of standing crystals is performed in a similar way; for reference, see Figure 9c. In the case of standing crystals the angle  $\alpha'$  between the  $y$ -direction and the projection of the transition moment corresponds to  $\varphi_i$ . Analogous to eq A.3, the fluorescence intensity at excitation in the  $x$ -direction can be calculated by

$$I_{\text{rel}}^x = \sum_{i=1}^6 |a|^4 \sin^2 \varphi_i \cos^2 \beta_i = \sin^4 \alpha \sum_{i=1}^6 \sin^2 \varphi_i \sin^2(\epsilon - \varphi_i) \quad (\text{A.6})$$

With the values of  $\varphi_i$  one obtains

$$I_{\text{rel}}^x = 3/2 \sin^4 \alpha [\sin^2(\epsilon - 60^\circ) + \sin^2(\epsilon - 120^\circ)] \quad (\text{A.7})$$

At linearly polarized excitation in the  $y$ -direction  $\sin^2 \varphi_i$  in eq A.6 is substituted by  $\cos^2 \varphi_i$ :

$$I_{\text{rel}}^y = \sum_{i=1}^6 |a|^4 \cos^2 \varphi_i \cos^2 \beta_i = \sin^4 \alpha \sum_{i=1}^6 \cos^2 \varphi_i \sin^2(\epsilon - \varphi_i) \quad (\text{A.8})$$

Thus the relative intensity can be calculated as

$$I_{\text{rel}}^y = 2 \sin^4 \alpha [\sin^2 \epsilon + 1/4 \sin^2(\epsilon - 60^\circ) + 1/4 \sin^2(\epsilon - 120^\circ)] \quad (\text{A.9})$$

## References and Notes

(1) Calzaferri, G.; Brühwiler, D.; Megelski, S.; Pfenniger, M.; Pauchard, M.; Hennessy, B.; Maas, H.; Devaux, A.; Graf, U. *Solid State Sci.* **2000**, *2*, 421.  
 (2) Pfenniger, M.; Calzaferri, G. *ChemPhysChem*, in press.

(3) Megelski, S. Dissertation, University of Bern, June 2000.  
 (4) Ernst, S.; Weitkamp, J. *Catal. Today* **1994**, *19*, 27.  
 (5) Tsapatsis, M.; Okubo, T.; Lovallo, M.; Davis, M. E. *Mater. Res. Soc. Symp. Proc.* **1995**, *371*, 21.  
 (6) Meng, X.; Zhang, Y.; Meng, C.; Pang, W. In *Proceedings of the 9th International Zeolite Conference, Montreal 1992*; Ballmoos, R., Ed.; Butterworth-Heinemann: New York, 1993.  
 (7) Barrer, R. M.; Villiger, H. Z. *Kristallogr.* **1969**, *128*, 352.  
 (8) Meier, W. M.; Olson, D. H.; Bärlocher, Ch. *Atlas Zeolite Struct. Types, Zeolites* **1996**, 17.  
 (9) Ohsuna, T.; Horikawa, Y.; Hiraga, K. *Chem. Mater.* **1998**, *10*, 688.  
 (10) Breck, D. W. *Zeolite Molecular Sieves*, John Wiley & Sons: New York, **1974**.  
 (11) Hennessy, B.; Megelski, S.; Marcolli, C.; Shklover, V.; Bärlocher, Ch.; Calzaferri, G. *J. Phys. Chem. B* **1999**, *103*, 3340.  
 (12) Calzaferri, G.; Gfeller, N. *J. Phys. Chem.* **1992**, *96*, 3428.  
 (13) Ramamurthy, V.; Sanderson, D.; Eaton, D. F. *J. Am. Chem. Soc.* **1993**, *115*, 10438.  
 (14) Pauchard M.; Devaux A.; Calzaferri G. *CHEM., A Eur. J.* **2000**, *6(18)*, 3456.  
 (15) Calzaferri, G. *Chimia* **1998**, *52*, 525.  
 (16) Schüth, F. *J. Phys. Chem.* **1992**, *96*, 7493.  
 (17) Binder, G.; Scandella, L.; Kritzenberger, J.; Gobrecht, J.; Koegler, J. H.; Prins, R. *J. Phys. Chem. B* **1997**, *101*, 483.  
 (18) Silbernagel, B. G.; Garcia, A. R.; Newsam, J. M. *Colloids Surf A* **1993**, *72*, 71.  
 (19) Newsam, J. M. *J. Phys. Chem.* **1989**, *93*, 7689.  
 (20) Gfeller, N.; Megelski, S.; Calzaferri, G. *J. Phys. Chem B* **1998**, *102*, 2433.  
 (21) Gfeller, N.; Megelski, S.; Calzaferri, G. *J. Phys. Chem B* **1999**, *103*, 1250.  
 (22) Gfeller, N.; Calzaferri, G. *J. Phys. Chem. B* **1997**, *101*, 1396.  
 (23) Bondi, A. *J. Phys. Chem.* **1964**, *68*, 441.  
 (24) *Proc. Int. Zeolite Conf., 12th Meeting* **1998**, *4*, 2839.  
 (25) Müller, B. R.; Calzaferri, G. *Micro. Mesop. Mater.* **1998**, *21*, 59.  
 (26) Lacowicz, J. R. *Principles of Fluorescence Spectroscopy*, 2nd ed.; Kluwer Academic/Plenum Publishers: New York, 1999.  
 (27) Bergamasco, S.; Calzaferri, G.; Hädener, K. *J. Photochem. Photobiol. A: Chem.* **1990**, *53*, 109.  
 (28) Bergamasco, S.; Calzaferri, G. *J. Photochem. Photobiol. A: Chem.* **1992**, *63*, 211.  
 (29) Fink, D. W.; Ohnesorge, W. E. *J. Phys. Chem.* **1970**, *74*, 72.  
 (30) Calzaferri G.; Rytz, R. *J. Phys. Chem.* **1995**, *99*, 12141.  
 (31) Weber, M. A. *Hochauflösende Lasermikroskopie an einzelnen Molekülen*. Ph.D. Thesis, University of Siegen, 1999; Franzbecker, Hildesheim, Germany, ISBN 3-88120-312-5.  
 (32) Weber, M. A.; Stracke, F.; Meixner, A. J. *J. Cytometry* **1999**, *36*, 217.  
 (33) Cerius, Release 1.6, Molecular Simulations, Burlington, 1995.  
 (34) Hoffmann, R. *J. Chem. Phys.* **1963**, *39*, 1397.  
 (35) Calzaferri, G.; Rytz, R.; Brändle, M.; Brühwiler, D.; Glaus, S. *ICON-EdiT, Extended Hückel Molecular Orbital and Transition Dipole Moment Calculations*; available at <http://iacrs1.unibe.ch>, 1999.  
 (36) Wolfsberg, M.; Helmholtz, L. *J. Chem. Phys.* **1952**, *20*, 837.  
 (37) Brühwiler, D.; Gfeller, N.; Calzaferri, G. *J. Phys. Chem. B* **1998**, *102*, 2923.  
 (38) (a) Pariser, R.; Parr, R. G. *J. Phys. Chem.* **1953**, *21*, 466, 767. (b) Pople, J. A.; *Trans. Faraday. Soc.* **1953**, *49*, 1375.  
 (39) Fabian, J.; Mehlhorn, A.; Zahradnik, R. *Theor. Chim. Acta* **1968**, *12*, 247.  
 (40) Preuss, E.; Linden, G.; Peuckert, M. *J. Phys. Chem.* **1985**, *89*, 2955.  
 (41) Förster, H.; Schuldt, M. *J. Chem. Phys.* **1977**, *66*, 5237.  
 (42) Böse, H.; Förster, H.; Fredé, W. *Chem. Phys. Lett.* **1987**, *138*, 401.  
 (43) Bordiga, S.; Garrone, E.; Lamberti, C.; Zecchina, A. F. *Chem. Soc., Faraday Trans.* **1994**, *90*, 3367.  
 (44) Renn, A.; Bucher, S.; Meixner, A. J.; Meister, E. C.; Wild, U. P. *J. Lumin.* **1988**, *39*, 181.